

Dinuclear Platinum(II) Complex Dominated by a Zig-Zag-Type Cyclometalated Ligand: An New Approach to Realize High-efficiency Near Infrared Emission

Shengyi Yang,^{a,b} Fanyuan Meng,^c Xiugang Wu,^b Zheng Yin,^{a,b} Xianzhi Liu,^{a,b} Caifa You,^{a,b} Yafei Wang,^{a,b*} Shijian Su,^{c,*} and Weiguo Zhu^{a,b*}

^a College of Chemistry, Xiangtan University, Key Lab of Environment-Friendly Chemistry and Application in Ministry of Education, Xiangtan 411105, China.

^b School of Materials Science and Engineering, Jiangsu Engineering Laboratory of Light-Electricity-Heat Energy-Converting Materials and Applications, Jiangsu Key Laboratories of Environment-Friendly Polymers, National Experimental Demonstration Center for Materials Science and Engineering, Changzhou University, Changzhou 213164, China.

^c Institute of Polymer Optoelectronic Materials and Devices, State Key Laboratory of Luminescent Materials and Devices, South China University of Technology, Guangzhou 510640, China

*Corresponding Authors

(W. Z) zhuwg18@126.com,

(S. S) mssjsu@scut.edu.cn,

(Y. W.) wangyf_miracle@hotmail.com

Captions of Figures

Fig. S1. ^1H NMR plot of BuPh-BDIQ

Fig. S2. ^{13}C NMR plot of BuPh-BDIQ

Fig. S3. MALDI-TOF-MS plot of BuPh-BDIQ

Fig. S4. ^1H NMR plot of (BuPh-BDIQ)Pt_{dpm}

Fig. S5. ^1H NMR plot of (BuPh-BDIQ)Pt_{2(dpm)}₂

Fig. S6. MALDI-TOF-MS plot of (BuPh-BDIQ)Pt_{dpm}

Fig. S7. MALDI-TOF-MS plot of (BuPh-BDIQ)Pt_{2(dpm)}₂

Fig. S8. Signal-crystal structures and molecular packing distance for (BuPh-BDIQ)Pt-dpm and (BuPh-BDIQ)Pt_{2(dpm)}₂

Fig. S9. Perspective view of (BuPh-BDIQ)Pt_{2(dpm)}₂ and (BuPh-BDIQ)Pt_{dpm}

Fig. S10. The dihedral angles between the auxiliary ligand and the rigid main ligand plane for (BuPh-BDIQ)Pt_{2(dpm)}₂ and (BuPh-BDIQ)Pt_{dpm}

Fig. S11. TGA curves of (BuPh-BDIQ)Pt_{dpm} and (BuPh-BDIQ)Pt_{2(dpm)}₂

Fig. S12. CV curves of (BuPh-BDIQ)Pt_{dpm} and (BuPh-BDIQ)Pt_{2(dpm)}₂

Fig. S13. Normalized UV-vis absorptions of (BuPh-BDIQ)Pt_{dpm} and (BuPh-BDIQ)Pt_{2-(dpm)}₂ in their toluene solutions and neat films

Fig. S14. PL spectra of (BuPh-BDIQ)Pt_{dpm} and (BuPh-BDIQ)Pt_{2(dpm)}₂ in their toluene solutions and neat films under air and N₂ atmosphere

Fig. S15. Room-temperature decay curves of (BuPh-BDIQ)Pt_{dpm} and (BuPh-BDIQ)Pt_{2-(dpm)}₂ in a dilute toluene solution

Fig. S16. Energy level diagram of (BuPh-BDIQ)Pt_{2(dpm)}₂

Fig. S17. Energy level diagram of (BuPh-BDIQ)Pt_{dpm}

Fig. S18. Device structure of the (BuPh-BDIQ)Pt_{dpm} and (BuPh-BDIQ)Pt_{2(dpm)}₂-doped light-emitting devices

Fig. S19. EL spectra of the (BuPh-BDIQ)Pt_{dpm} doped PLEDs at different doping concentrations of 1wt%, 2 wt%, 4 wt% and 8 wt%

Fig. S20. EL spectra of the (BuPh-BDIQ)Pt_{2(dpm)}₂ doped PLEDs at different doping concentrations of 1wt%, 2 wt%, 4 wt% and 8 wt%

Fig. S21. *EQE-J* curves of the (BuPh-BDIQ)Pt_{dpm} doped PLEDs at different doping concentrations of 1wt%, 2 wt%, 4 wt% and 8 wt%

Fig. S22. *EQE-J* curves of the (BuPh-BDIQ)Pt_{2(dpm)}₂ doped PLEDs at different doping concentrations of 1wt%, 2 wt%, 4 wt% and 8 wt%

Fig. S23. *J-V-R* curves of the (BuPh-BDIQ)Pt_{dpm} doped PLEDs at different doping concentrations of 1wt%, 2 wt%, 4 wt% and 8 wt%

Fig. S24. *J-V-R* curves of the (BuPh-BDIQ)Pt_{2(dpm)}₂ doped PLEDs at different doping concentrations of 1wt%, 2 wt%, 4 wt% and 8 wt%

Table S1. Rate constants K_r and K_{nr} of (BuPh-BDIQ)Pt_{dpm} and (BuPh-BDIQ)-Pt_{2(dpm)}₂

Table S2. Selected TD-DFT results of (BuPh-BDIQ)Pt_{2(dpm)}₂

Table S3. Selected TD-DFT results of (BuPh-BDIQ)Pt_{dpm}

Table S4. *EQE* and *J-V-R* data of the (BuPh-BDIQ)Pt_{dpm} and (BuPh-BDIQ)Pt_{2(dpm)}₂ doped PLEDs

Table S5. The maximum of EL wavelength, *EQE* and irradiance summary of the representative NIR-emitting dinuclear platinum complexes

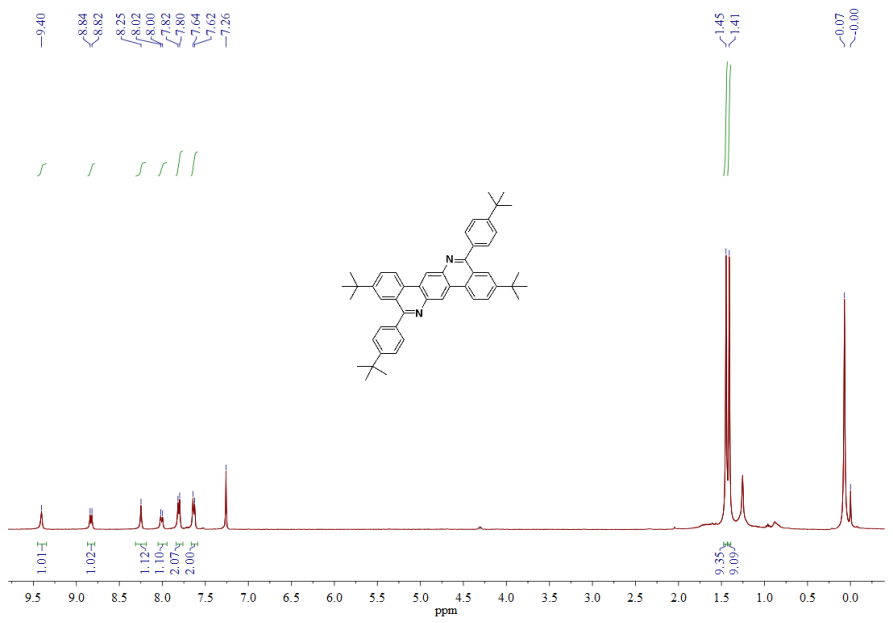


Fig. S1. ¹H NMR plot ofBuPh-BDIQ

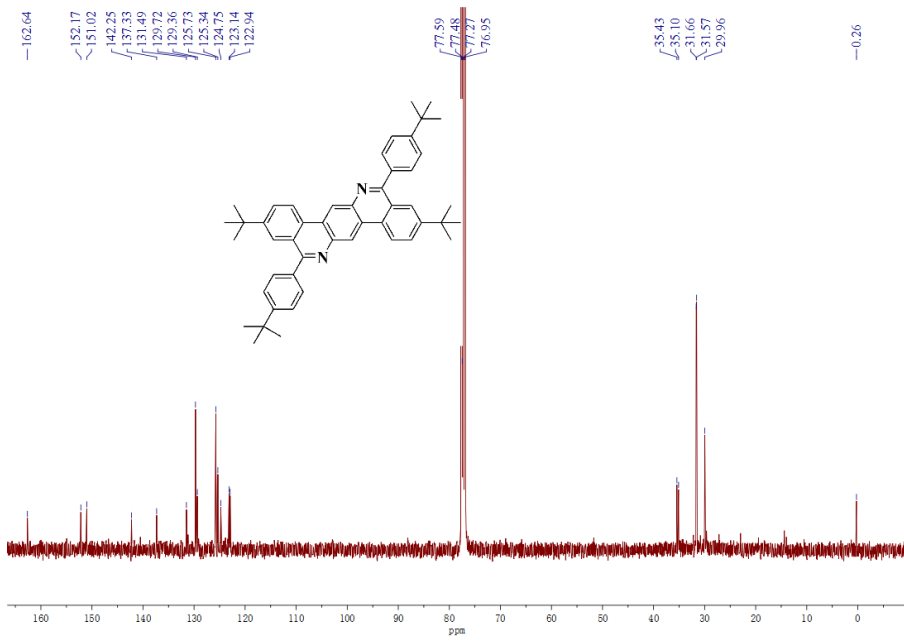


Fig. S2. ¹³C NMR plot ofBuPh-BDIQ

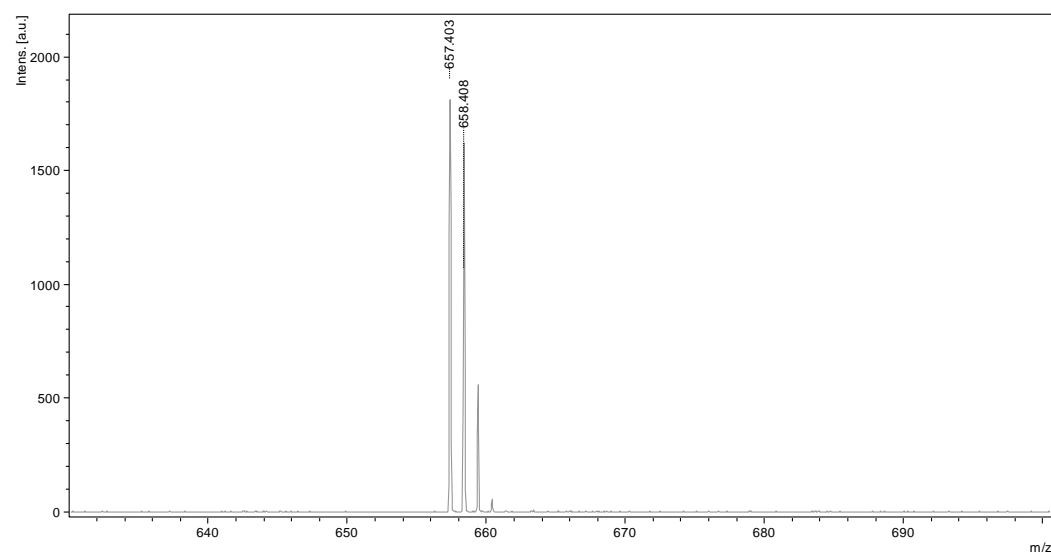


Fig. S3. MALDI-TOF-MS plot of BuPh-BDIQ

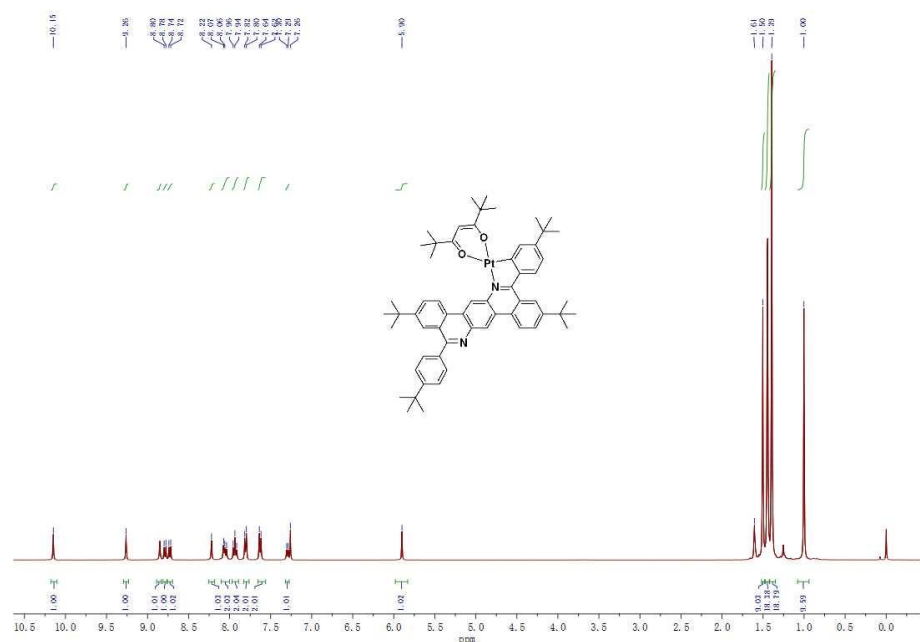


Fig. S4. ^1H NMR plot of (BuPh-BDIQ)Ptdpm

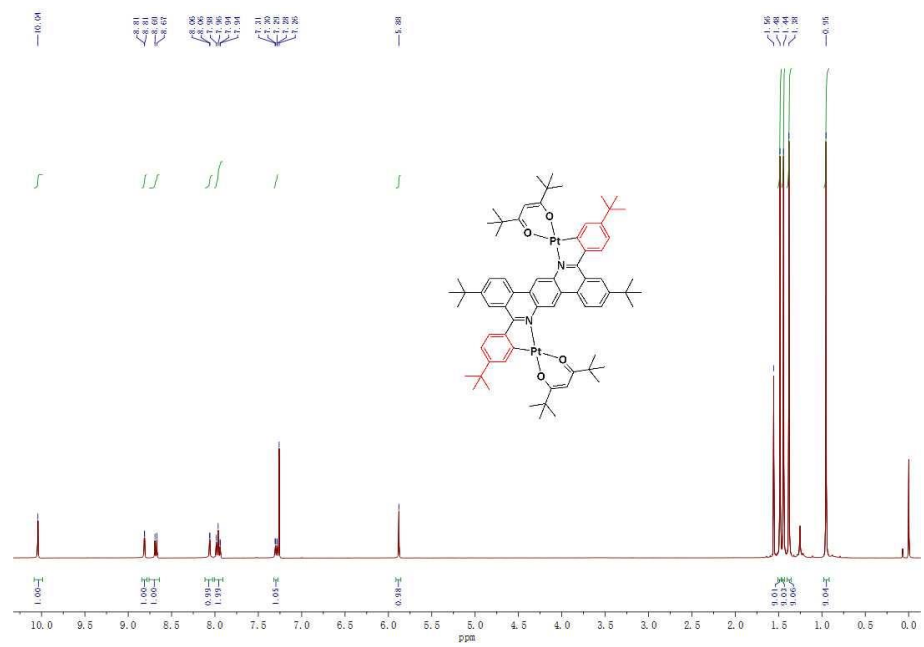


Fig. S5. ^1H NMR plot of (BuPh-BDIQ)Pt₂(dpm)₂

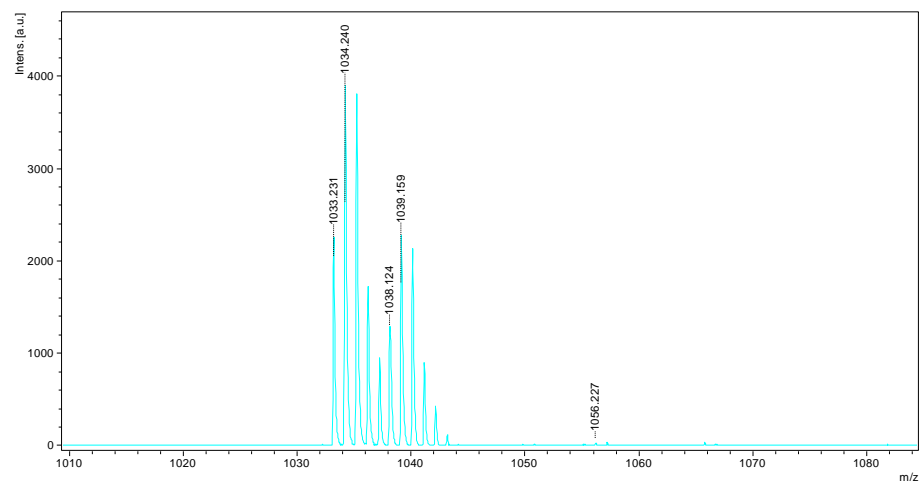


Fig. S6. MALDI-TOF-MS plot of (BuPh-BDIQ)Ptdpm

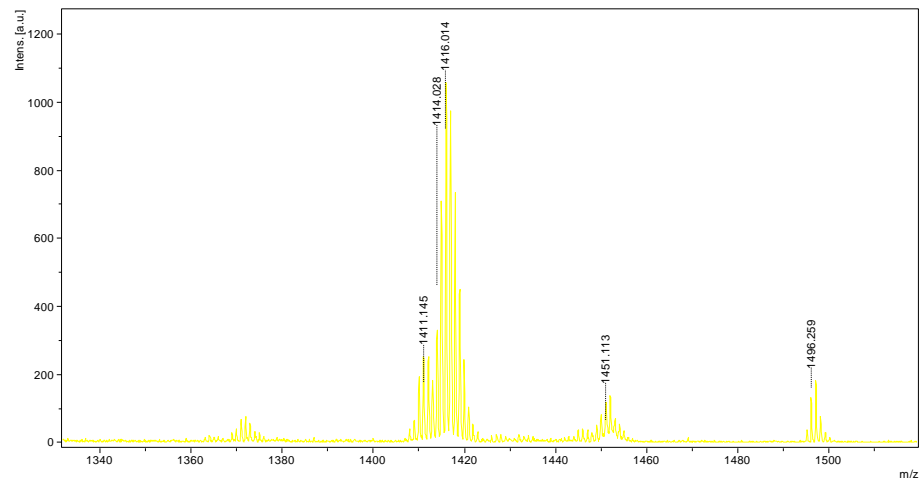


Fig. S7. MALDI-TOF-MS plot of $(\text{BuPh}-\text{BDIQ})\text{Pt}_2(\text{dpm})_2$

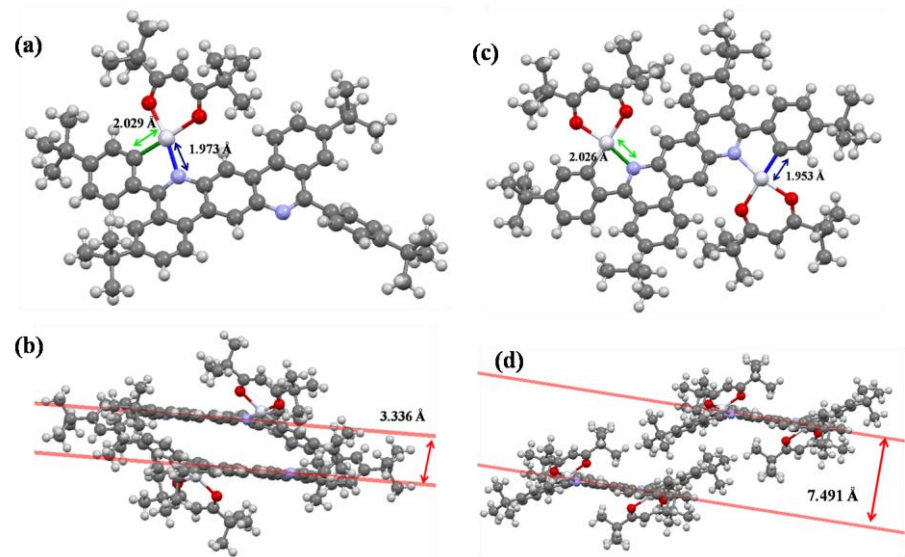


Fig. S8. Signal-crystal structures and molecular packing distance for $(\text{BuPh}-\text{BDIQ})\text{Ptdpm}$ (a and b) and $(\text{BuPh}-\text{BDIQ})\text{Pt}_2(\text{dpm})_2$ (c and d)

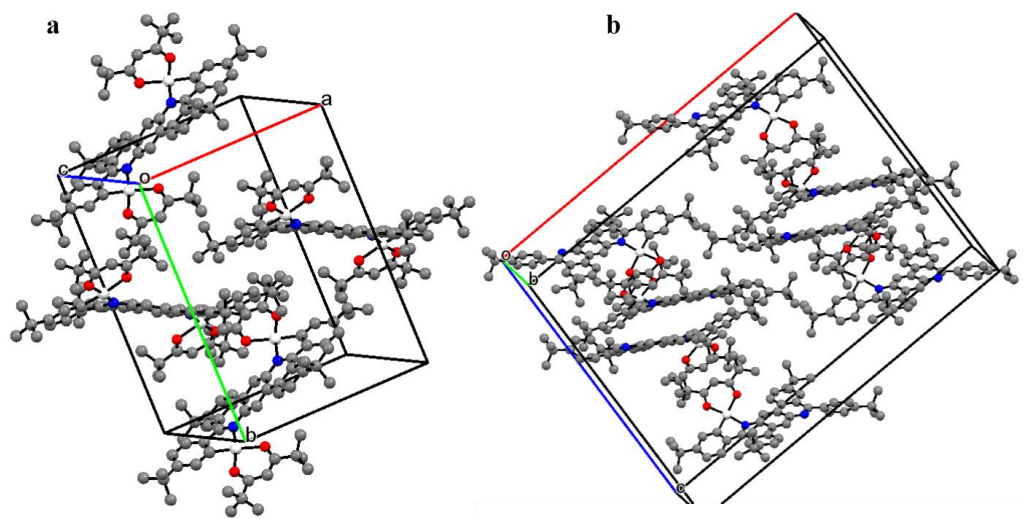


Fig. S9. Perspective view of $(\text{BuPh-BDIQ})\text{Pt}_2(\text{dpm})_2$ and $(\text{BuPh-BDIQ})\text{Ptdpm}$

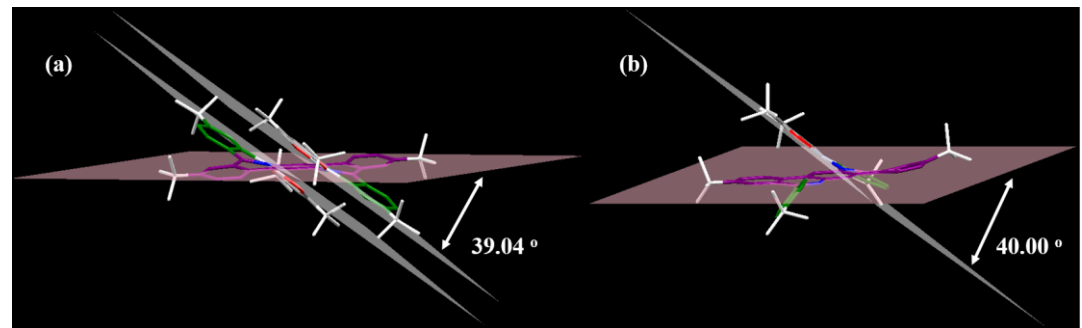


Fig. S10. The dihedral angles between the auxiliary ligand and the rigid main ligand plane for (a) $(\text{BuPh-BDIQ})\text{Pt}_2(\text{dpm})_2$ and (b) $(\text{BuPh-BDIQ})\text{Ptdpm}$

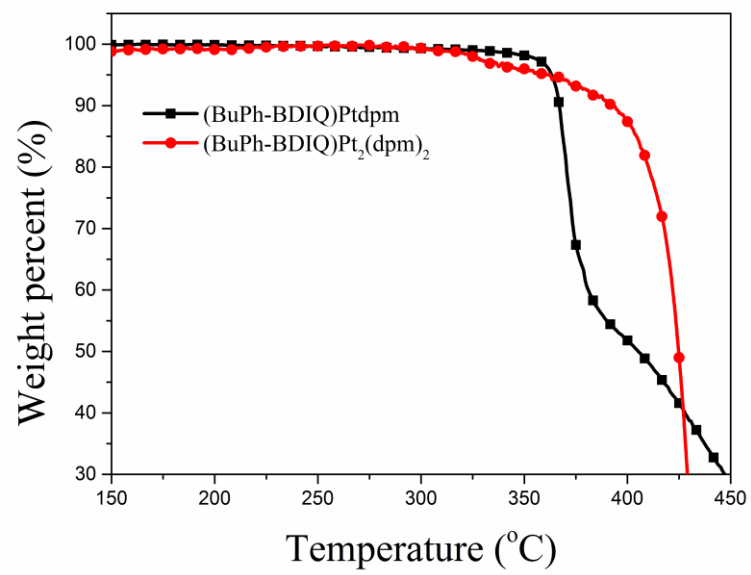


Fig. S11. TGA curves of $(\text{BuPh-BDIQ})\text{Pt dpmm}$ and $(\text{BuPh-BDIQ})\text{Pt}_2(\text{dpm})_2$

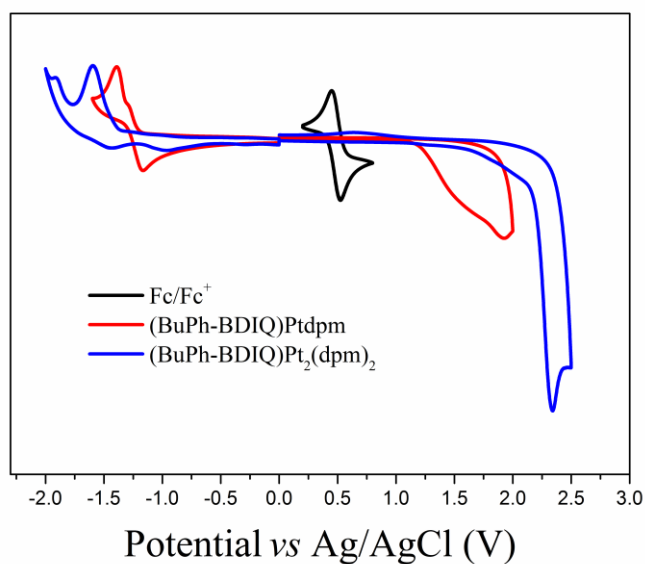


Fig. S12. CV curves of $(\text{BuPh-BDIQ})\text{Pt dpmm}$ and $(\text{BuPh-BDIQ})\text{Pt}_2(\text{dpm})_2$

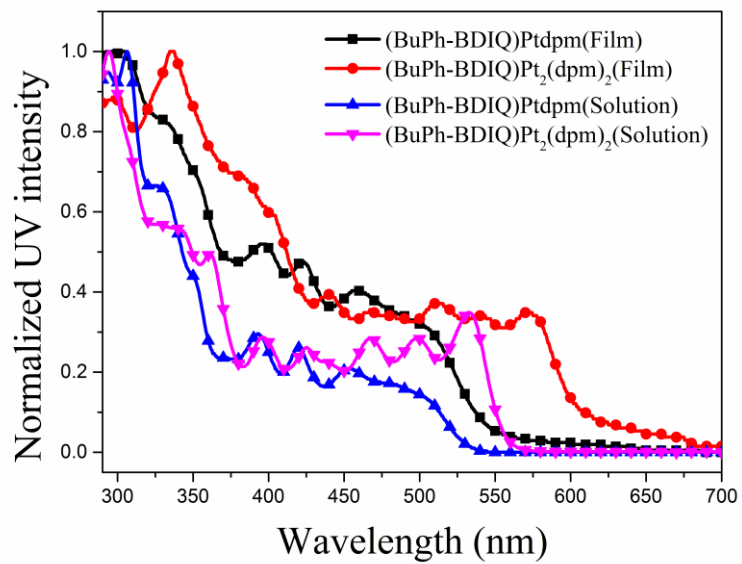


Fig. S13. Normalized UV-vis absorptions of (BuPh-BDIQ)Ptdpm and (BuPh-BDIQ)Pt₂(dpm)₂ in their toluene solutions and neat films.

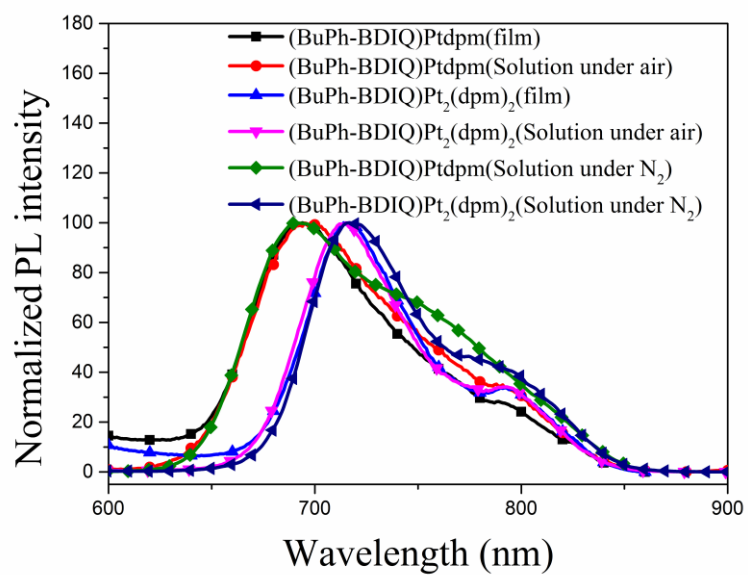


Fig. S14. PL spectra of (BuPh-BDIQ)Ptdpm and (BuPh-BDIQ)Pt₂(dpm)₂ in their toluene solutions and neat films under air and N₂ atmosphere

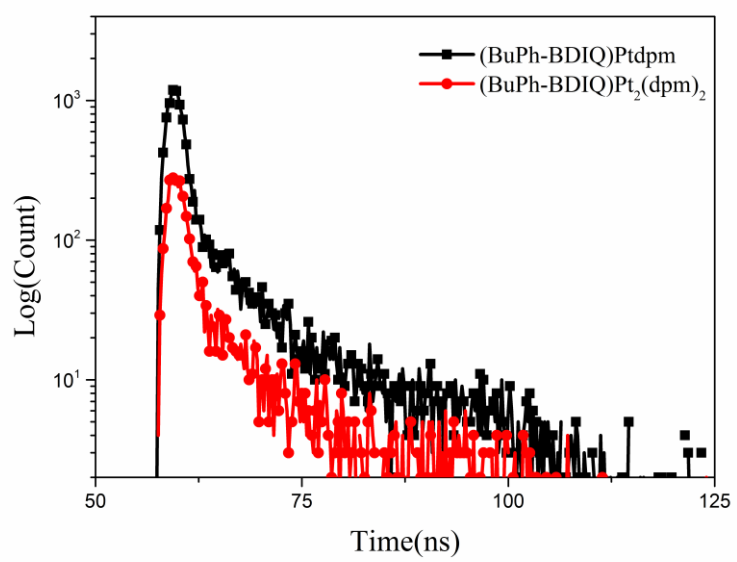


Fig. S15. Room-temperature decay curves of both platinum complexes in a dilute toluene solution

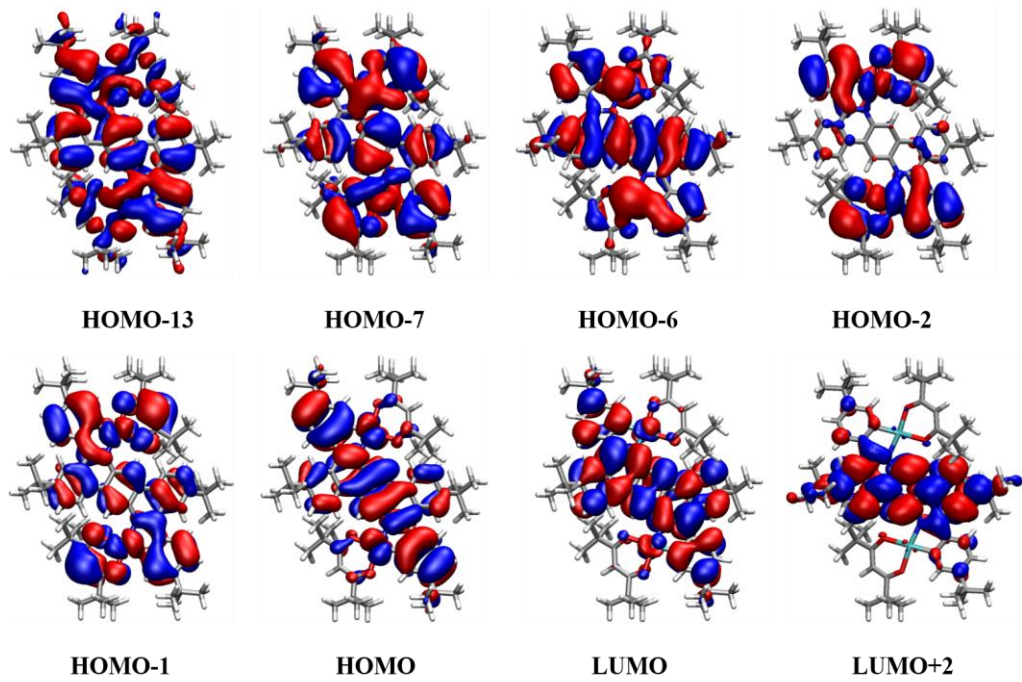


Fig. S16. Energy level diagram of (BuPh-BDIQ)Pt₂(dpm)₂

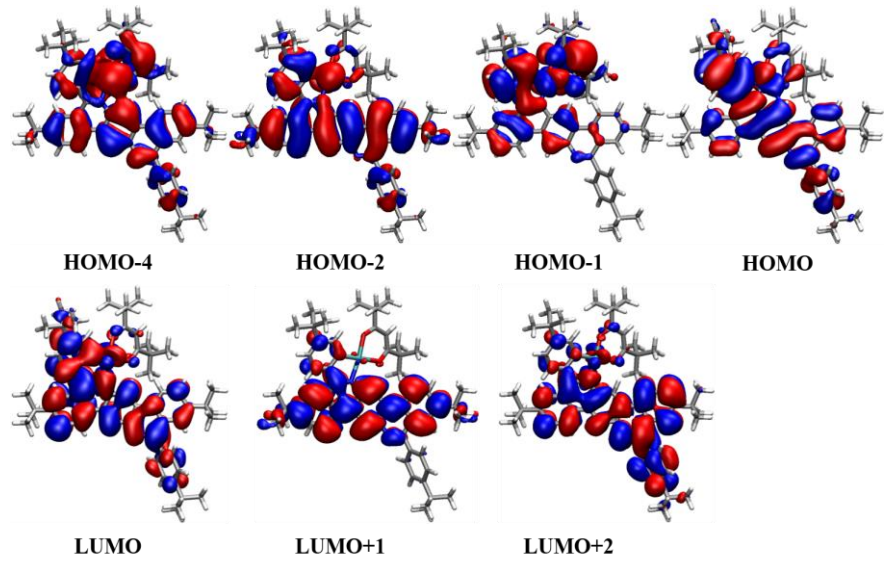


Fig. S17. Energy level diagram of (BuPh-BDIQ)Ptdpm

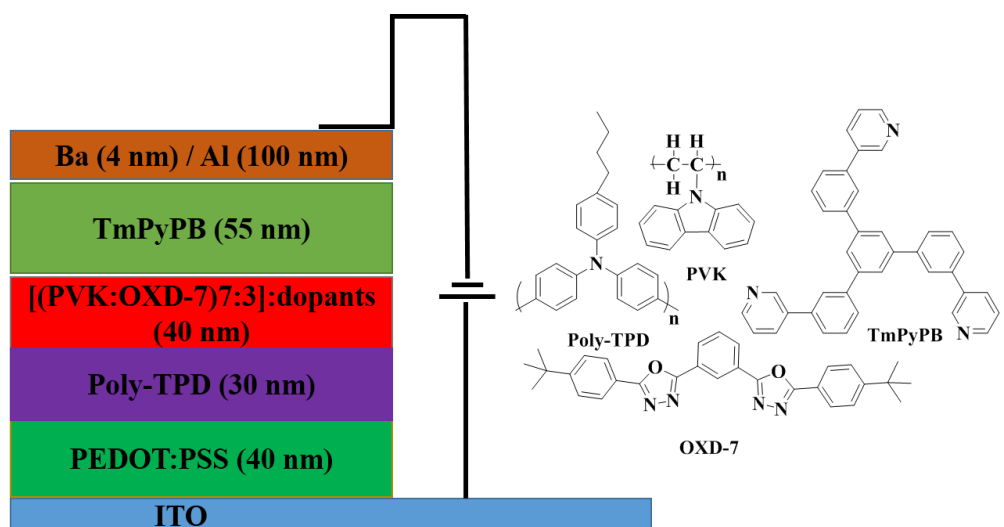


Fig. S18. Device structure of the (BuPh-BDIQ)Ptdpm and (BuPh-BDIQ)Pt₂(dpm)₂-doped devices

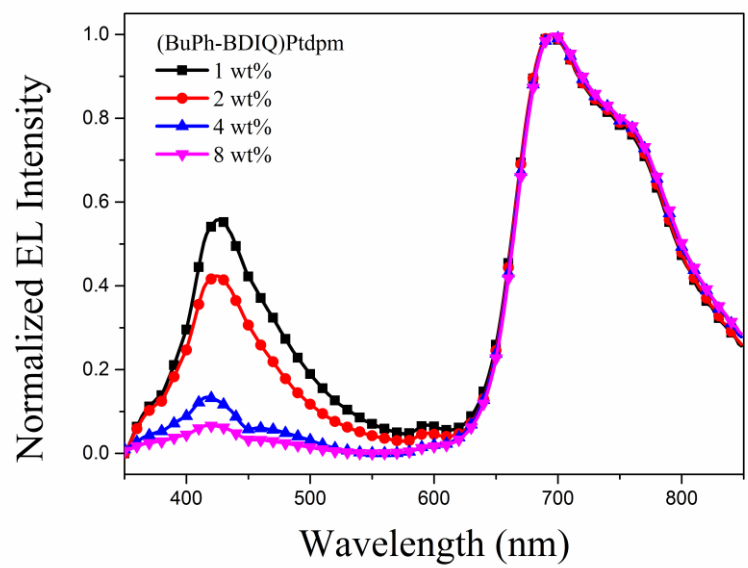


Fig. S19. EL spectra of the (BuPh-BDIQ)Ptdpm doped devices at different doping concentrations of 1wt%, 2 wt%, 4 wt% and 8 wt%

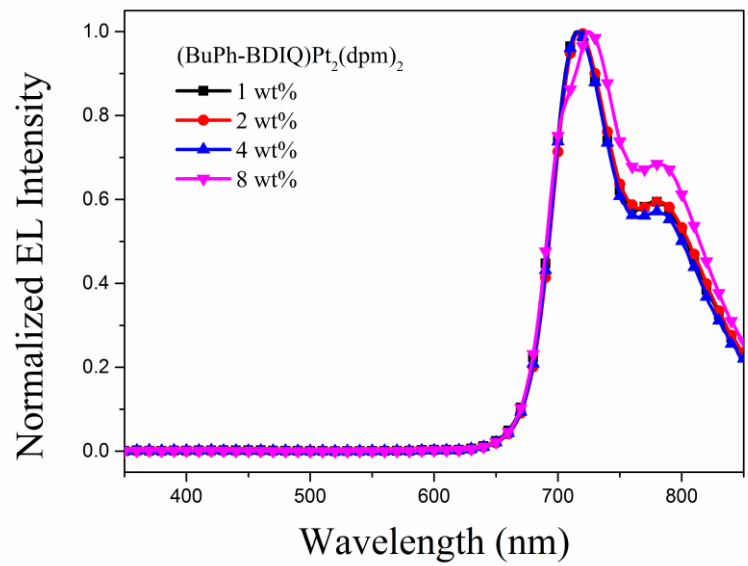


Fig. S20. EL spectra of the (BuPh-BDIQ)Pt₂(dpm)₂ doped PLEDs at different doping concentrations of 1wt%, 2 wt%, 4 wt% and 8 wt%

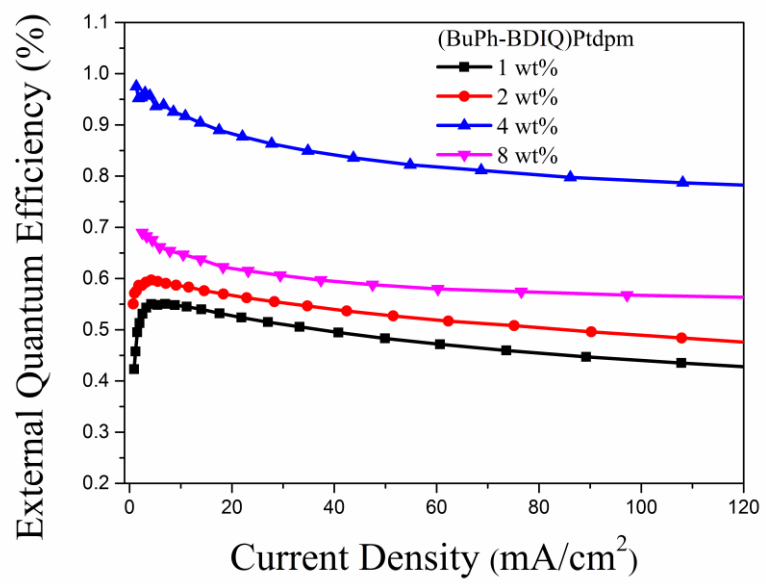


Fig. S21. EQE-*J* curves of the (BuPh-BDIQ)Ptdpm doped PLEDs at different doping concentrations of 1wt%, 2 wt%, 4 wt% and 8 wt%

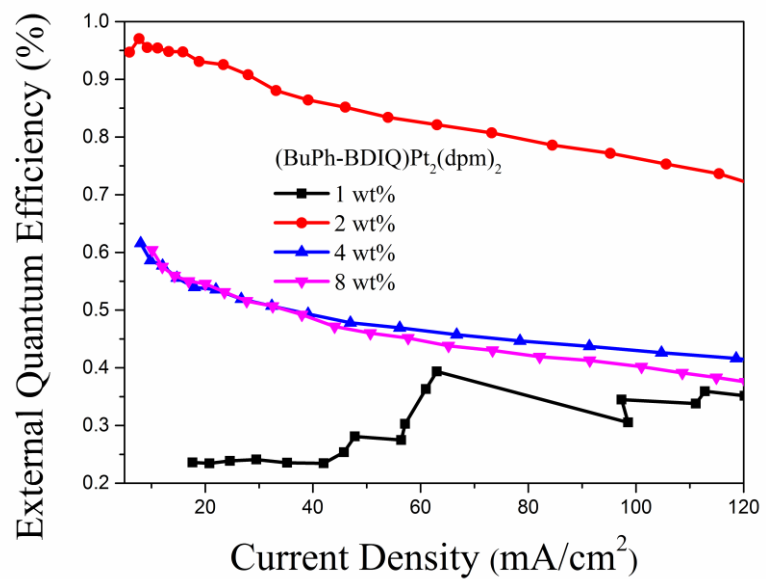


Fig. S22. EQE-*J* curves of the (BuPh-BDIQ)Pt₂(dpm)₂ doped PLEDs at different doping concentrations of 1wt%, 2 wt%, 4 wt% and 8 wt%

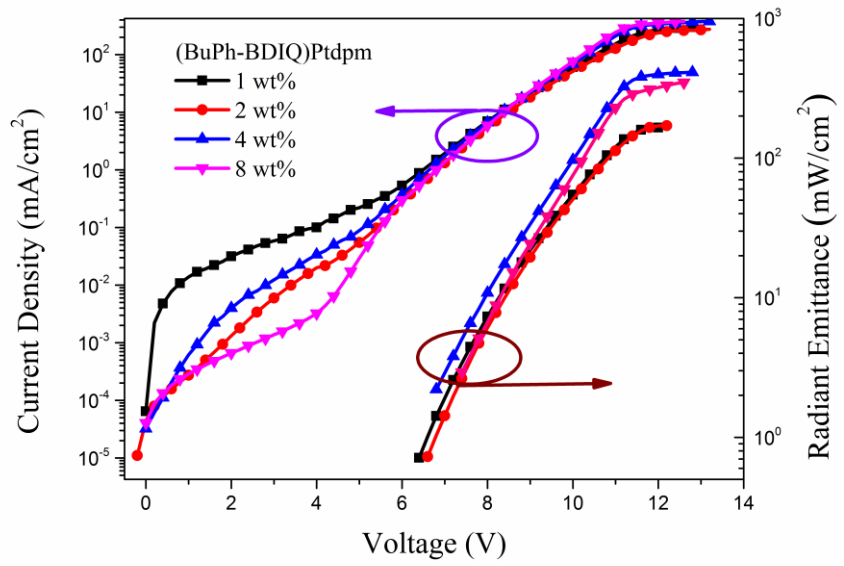


Fig. S23. *J-V-R* curves of the (BuPh-BDIQ)Ptdpm doped PLEDs at different doping concentrations of 1wt%, 2 wt%, 4 wt% and 8 wt%

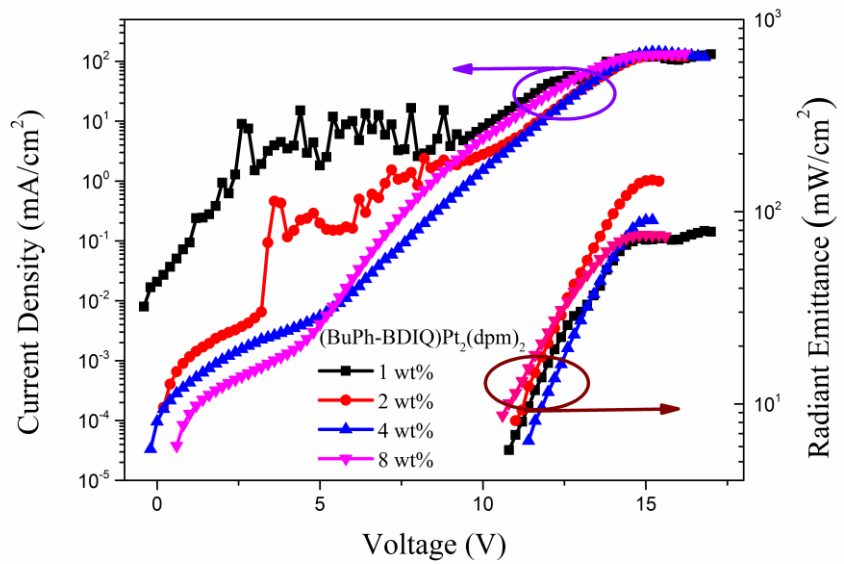


Fig. S24. *J-V-R* curves of the (BuPh-BDIQ)Pt₂(dpm)₂ doped PLEDs at different doping concentrations of 1wt%, 2 wt%, 4 wt% and 8 wt%

Table S1. Rate constants K_r and K_{nr} of (BuPh-BDIQ)Pt_{dpm} and (BuPh-BDIQ)Pt_{2(dpm)}₂

Complexes	$K_r [10^5 \text{ s}^{-1}]^a$	$K_{nr} [10^5 \text{ s}^{-1}]^a$
(BuPh-BDIQ)Pt _{dpm}	0.0237	6.555
(BuPh-BDIQ)Pt _{2(dpm)} ₂	0.2129	5.635

^aRate constants K_r and K_{nr} are calculated using the equations $K_r = \Phi_f/\tau$ and $K_{nr} = (1 - \Phi_f)/\tau$.

Table S2. Selected TD-DFT results of (BuPh-BDIQ)Pt_{2(dpm)}₂

NO.	State	λ/nm	f	Transition
1	S1	517	0.3377	HOMO-2 → LUMO +1 (2.1%) HOMO-1 → LUMO (4.9%) HOMO → LUMO (88.9%)
2	S3	468	0.1087	HOMO-1 → LUMO (90.7%) HOMO → LUMO (4.8%)
3	S7	412	0.0921	HOMO-7 → LUMO (2.4%) HOMO-6 → LUMO (52.7%) HOMO-4 → LUMO (21.4%) HOMO → LUMO+2 (16.6%)
4	S12	371	0.1820	HOMO-6 → LUMO (6.7%) HOMO-4 → LUMO (9.0%) HOMO-3 → LUMO+1 (10.4%) HOMO → LUMO+2 (68.1%)
5	S15	353	0.2119	HOMO-2 → LUMO+2 (96.1%)
6	S27	327	0.1062	HOMO-13 → LUMO (43.0%) HOMO-10 → LUMO (8.9%) HOMO-8 → LUMO+1 (2.7%) HOMO-4 → LUMO+2 (5.8%) HOMO-2 → LUMO+4 (4.7%) HOMO → LUMO+3 (25.2%)
7	S40	298	0.5285	HOMO-15 → LUMO (8.7%) HOMO-7 → LUMO+2 (49.8%) HOMO-6 → LUMO+2 (7.9%) HOMO-4 → LUMO+2 (11.8%)

Table S3. Selected TD-DFT results of (BuPh-BDIQ)Ptdpm

NO.	State	λ/nm	f	Transition
1	S1	482	0.1902	HOMO-1→LUMO (11.7%)
				HOMO→LUMO (80.9%)
2	S2	449	0.1012	HOMO-1→LUMO (85.1%)
				HOMO→LUMO (9.7%)
3	S4	403	0.1501	HOMO-4→LUMO (8.2%)
				HOMO-3→LUMO (8.9%)
				HOMO-2→LUMO (62.2%)
				HOMO→LUMO+1 (13.1%)
4	S5	390	0.1800	HOMO-4→LUMO (51.2%)
				HOMO-3→LUMO (38.0%)
				HOMO→LUMO (4.0%)
				HOMO→LUMO+1 (2.4%)
S8		346	0.1983	HOMO-5→LUMO (12.0%)
				HOMO-2→LUMO (2.3%)
				HOMO-1→LUMO+1 (75.6%)
5		346	0.1983	HOMO→LUMO+2 (2.6%)
				HOMO-1→LUMO+1 (4.8%)
				HOMO→LUMO+1 (2.4%)
S9				HOMO→LUMO+2 (80.3%)

Table S4. The EQE and $J-V-R$ data of the (BuPh-BDIQ)Ptdpm and (BuPh-BDIQ)Pt₂(dpm)₂ doped PLEDs

Complexes	Doping concentrations	V_{on} (V)	λ_{EL} (nm)	R ($\mu\text{W}/\text{cm}^2$)	EQE_{max} (%)
(BuPh-BDIQ)Ptdpm	1 wt%	6.4	694	165	0.55
	2 wt%	6.6	694	171	0.60
	4 wt%	6.8	696	412	0.97
	8 wt%	7.4	696	348	0.69
(BuPh-BDIQ)Pt ₂ (dpm) ₂	1 wt%	11.0	716	79	0.39
	2 wt%	11.2	718	146	0.97
	4 wt%	11.6	724	90	0.62
	8 wt%	10.8	716	76	0.60

Table S5. The maximum of EL wavelength, EQE and irradiance summary of the representative NIR dinuclear platinum complexes

Compound	Structure	EL_{max} (nm)	EQE_{max} (%)	R_{max} $\mu\text{W}/\text{cm}^2$	Ref.
This work: (BuPh-BDIQ)Pt ₂ (dpm) ₂		785	0.97	146	-
Fl(TPA-BTPy) ₂ Pt ₂ (pic) ₂		780	0.02	59	1
(BuPyrDPy)[Pt(dpm)] ₂		762	0.31	26.9	2

1 Y. M. Zhang, F. Meng, J. H. Tang, Y. Wang, C. You, H. Tan, Y. Liu, Y. W. Zhong, S. Su and W. Zhu, Dalton Trans, 2016, **45**, 5071-5080.

2 Z. Hao, F. Meng, P. Wang, Y. Wang, H. Tan, Y. Pei, S. Su and Y. Liu, Dalton Trans, 2017, **46**, 16257-16268.